

Supersymmetric Box Contributions to $e^+e^- \rightarrow Z^0h^0$ and $e^+e^- \rightarrow A^0h^0$.

Volker DRIESEN and Wolfgang HOLLIK

Institut für Theoretische Physik
Universität Karlsruhe
Kaiserstr. 12, Postfach 6980
D-76128 Karlsruhe, Germany

Abstract

Within the MSSM we calculate the electroweak 1-loop box contributions to the processes $e^+e^- \rightarrow Z^0h^0$ and $e^+e^- \rightarrow A^0h^0$. We present detailed results for c. m. energies $\sqrt{s} = 200$ GeV and $\sqrt{s} = 500$ GeV as well as for $\tan\beta = 2$ and $\tan\beta = 50$. The box contributions to the process $e^+e^- \rightarrow Z^0h^0$ are, depending on \sqrt{s} and $\tan\beta$, of the order -2 to -20% and to $e^+e^- \rightarrow A^0h^0$ of 2 to 10%.

1 Introduction

Experiments at the forthcoming upgrade of the LEP collider to LEP2 will continue the search for Higgs bosons in the mass range up to 100-110 GeV [1], depending on the energy and luminosity at this machine. Besides the search for the Standard Model Higgs boson, numerous studies are devoted to the Higgs bosons of the minimal supersymmetric standard model (MSSM) [2], the most predictive framework beyond the Standard Model, where at least one light neutral scalar with mass $\lesssim 130$ GeV is expected. This mass range can be fully explored at new e^+e^- colliders with energies up to 500 GeV [2, 7]. Detailed studies of Higgs production and decay processes are required to detect the possible signals of Higgs bosons and to distinguish as far as possible the origin of a produced scalar particle. The most promising process to search for the standard Higgs boson is the bremsstrahlung type reaction $e^+e^- \rightarrow ZH$ at energies $> M_H + M_Z$. For Higgs bosons of the MSSM the basic production channels are

$$e^+e^- \rightarrow Zh^0 \tag{Z}$$

and

$$e^+e^- \rightarrow A^0h^0 \tag{A}$$

where h^0 is the lightest CP even and A^0 the CP odd neutral particle of the MSSM Higgs spectrum.

For an accurate discussion of the production cross sections one has to include radiative corrections. For the standard Higgs complete 1-loop calculations for $e^+e^- \rightarrow ZH$ are available [3]. For the corresponding processes in the MSSM no complete 1-loop calculation has been performed so far. Besides the approximate methods of the effective potential approach [4] and the renormalization group treatment [5] it is of particular interest to also have a complete diagrammatic calculation:

- it allows for all virtual particle effects within the MSSM without restrictions to masses and mixings,
- it takes into account all momentum dependent effects in 2- and 3- point functions,
- it provides a reference frame for checking the quality of simpler compact approximations which might be useful for practical applications.

The complete set of 1-loop diagrams contributing to the MSSM neutral Higgs production processes is very extensive, and until now only one calculation has been carried out [6] based on the following building blocks: the set of self energy corrections to the vector boson and Higgs propagators and wave functions, the vertex corrections to the e^+e^-Z , ZZh , ZAh vertices, and the corresponding counter terms in the on-shell renormalization scheme. The box diagram contributions have not yet been considered so far, and they are also not part of the phenomenological studies for LEP2 and higher energy colliders [7, 8].

In this paper we provide the box contributions to both $e^+e^- \rightarrow Zh$ and $e^+e^- \rightarrow Ah$. Box diagrams are required for theoretical reasons to render the amplitudes gauge independent, and for practical reasons since they are in general of non-negligible size. The computation in [6] on the basis of 2- and 3-point functions was performed in the 't Hooft-Feynman gauge with $\xi = 1$. In this specific gauge, the box contributions are finite and independent of the details of the renormalization. Hence, we proceed to derive the box contribution in the $R_{\xi=1}$ gauge as well, thus providing the missing ingredients as an independent, finite and scheme independent block for completing the amplitudes and cross sections.

2 Cross Sections

The Born diagrams contributing to process (Z) and (A) are displayed in Fig. 1 together with the momentum assignment. p_3 always denotes the outgoing h^0 momentum, whereas p_4 is the momentum of the outgoing Z or A^0 , respectively. ε_Z^μ denotes the polarization vector of the Z . Furthermore, we use the invariant variables

$$s = (p_1 + p_2)^2, \quad t = (p_1 - p_3)^2, \quad u = (p_1 - p_4)^2$$

and the scattering angle $\theta = \angle(e^-, h^0)$ in the c. m. system. The masses of e^+ and e^- have been neglected for the entire calculation.

Including the box diagrams (Fig. 2 and 3) one has to take into account their interference with the corresponding Born amplitudes. The differential cross section in the c. m. system can be written in the following way:

$$\frac{d\sigma_Z}{d\cos\theta} = \frac{\sqrt{\lambda(s, M_Z^2, M_h^2)}}{32\pi s^2} \left(T_Z^0 + \sum_n T_Z^n \right) \quad (1)$$

$$\frac{d\sigma_A}{d\cos\theta} = \frac{\sqrt{\lambda(s, M_A^2, M_h^2)}}{32\pi s^2} \left(T_A^0 + \sum_l T_A^l \right) \quad (2)$$

with $\lambda(x, y, z) = x^2 + y^2 + z^2 - 2(xy + xz + yz)$. The index n counts the diagrams of Fig. 2, and l those of Fig. 3. Thereby it is understood that the summation is performed also over the various $\tilde{\chi}^0$ and $\tilde{\chi}^+$ states as well as over \tilde{e}_L and \tilde{e}_R .

$T_{Z,A}^0$ denote the lowest order contributions following from the Born amplitudes

$$\mathcal{M}_{Z,A}^0 = \bar{v}(p_2) \mathcal{O}_{Z,A}^0 u(p_1) \quad (3)$$

with

$$\mathcal{O}_Z^0 = i \frac{g^2 M_Z^2 \sin(\beta - \alpha)}{c_w^2 (s - M_Z^2)} \gamma_\mu \left[(g_V^e + g_A^e) \mathcal{P}_L + (g_V^e - g_A^e) \mathcal{P}_R \right] \varepsilon_Z^\mu(\sigma) \quad (4)$$

for process (Z), and

$$\mathcal{O}_A^0 = - \frac{g^2 \cos(\beta - \alpha)}{2 c_w^2 (s - M_Z^2)} \gamma_\mu \left[(g_V^e + g_A^e) \mathcal{P}_L + (g_V^e - g_A^e) \mathcal{P}_R \right] (p_3 - p_4)^\mu \quad (5)$$

for process (A), where

$$g_V^e = -\frac{1}{4} + s_w^2, \quad g_A^e = -\frac{1}{4} \quad (6)$$

are the standard NC couplings, $g = e/s_w$, and α, β the mixing angles of the Higgs sector.

Averaging over the initial helicities for unpolarized e^\pm and summing over the Z polarizations σ in case of (Z) yield the following expressions

$$T_Z^0 = \frac{1}{4} \sum_{\sigma} \text{Tr} (\not{p}_2 \mathcal{O}_Z^0 \not{p}_1 \bar{\mathcal{O}}_Z^0) \quad (7)$$

$$T_A^0 = \frac{1}{4} \text{Tr} (\not{p}_2 \mathcal{O}_A^0 \not{p}_1 \bar{\mathcal{O}}_A^0) \quad (8)$$

which result in the explicit forms of the Born cross sections:

$$\frac{d\sigma_Z^0}{d\cos\theta} = \frac{1}{128\pi s^2} \frac{g^4}{c_w^4} \sin^2(\beta - \alpha) \frac{\sqrt{\lambda(s, M_Z^2, M_h^2)}}{(s - M_Z^2)^2} (g_V^{e^2} + g_A^{e^2})^2 2 (t u + 2sM_Z^2 - M_Z^2 M_h^2) \quad (9)$$

$$\frac{d\sigma_A^0}{d\cos\theta} = \frac{1}{128\pi s^2} \frac{g^4}{c_w^4} \cos^2(\beta - \alpha) \frac{\sqrt{\lambda(s, M_A^2, M_h^2)}}{(s - M_Z^2)^2} (g_V^{e^2} + g_A^{e^2})^2 2 (t u - M_A^2 M_h^2) \quad (10)$$

The interference terms in (1), (2) can be expressed in a way analogous to (7,8):

$$T_Z^n = \frac{1}{2} \sum_{\sigma} \text{Re} [\text{Tr} (\not{p}_2 \mathcal{O}_Z^n \not{p}_1 \bar{\mathcal{O}}_Z^0)] \quad (11)$$

$$T_A^l = \frac{1}{2} \text{Re} [\text{Tr} (\not{p}_2 \mathcal{O}_A^l \not{p}_1 \bar{\mathcal{O}}_A^0)] \quad (12)$$

with the operators \mathcal{O}_Z^n corresponding to the diagrams of Fig. 2 and \mathcal{O}_A^l to those of Fig. 3.

For the discussion of the various contributions it is useful to distinguish between the genuine SUSY diagrams with virtual selectrons (se) and sneutrinos (snu) and the residual diagrams of the standard model with 2 Higgs doublets (2hdm):

Figure 2:

$$\begin{aligned} \mathcal{O}_Z^{\text{se}} &= \text{diagrams}(1, 2, 3) + (h \leftrightarrow Z) \\ \mathcal{O}_Z^{\text{snu}} &= \text{diagrams}(4, 5, 6) + (h \leftrightarrow Z) \\ \mathcal{O}_Z^{\text{2hdm}} &= \text{diagrams}(7, 8) + (h \leftrightarrow Z) + \text{diagrams}(9, 10) \end{aligned} \quad (13)$$

Figure 3:

$$\begin{aligned} \mathcal{O}_A^{\text{se}} &= \text{diagram 2} + (h \leftrightarrow A) + \text{diagram 4} \\ \mathcal{O}_A^{\text{snu}} &= \text{diagram 3} + (h \leftrightarrow A) + \text{diagram 5} \\ \mathcal{O}_A^{\text{2hdm}} &= \text{diagram 1} + (h \leftrightarrow A) \end{aligned} \quad (14)$$

including summation over the $\tilde{\chi}^0, \tilde{\chi}^+$, and $\tilde{e}_{L,R}$ states.

Our conventions for the Feynman rules are adopted from ref. [9] and for fermion number violating processes from ref. [10]. The calculations were done using the algebraic program FORM [11] and the package FF [12] to evaluate the tensor integrals.

According to the decomposition (13,14) we can write for the cross sections:

$$\frac{d\sigma_{Z,A}}{d\cos\theta} = \frac{d\sigma_{Z,A}^0}{d\cos\theta} \left[1 + \delta_{Z,A}^{\text{box}} \right] \quad (15)$$

with the relative box contribution

$$\delta_{Z,A}^{\text{box}} = \delta_{Z,A}^{2\text{hdm}} + \delta_{Z,A}^{\text{se}} + \delta_{Z,A}^{\text{snu}}. \quad (16)$$

In a similar way we express the integrated cross sections as

$$\sigma_{Z,A} = \sigma_{Z,A}^0 \left[1 + \Delta_{Z,A}^{\text{box}} \right] \quad (17)$$

with

$$\Delta_{Z,A}^{\text{box}} = \Delta_{Z,A}^{2\text{hdm}} + \Delta_{Z,A}^{\text{se}} + \Delta_{Z,A}^{\text{snu}} \quad (18)$$

where $\sigma_{Z,A}^0$ denote the Born terms following from (9) and (10) by integration over $\cos\theta$.

3 Results and discussion

In this section we present and discuss the numerical influence of the box diagrams on the production cross sections. As concrete examples we have chosen two sets of Higgs masses where both Zh^0 and A^0h^0 can be produced at LEP2 energies. Taking $M_A = 90$ GeV, one has $M_h = 40$ GeV for $\tan\beta = 2$ and $M_h = 89$ GeV for $\tan\beta = 50$. These mass values correspond to the lowest order MSSM Higgs spectrum. At this stage we have not yet included higher order effects since that would include a bunch of additional parameters like m_t , scalar top masses and mixing parameters which are not directly related to the specific problems addressed in this note. The input required for calculating the box contributions is M_h and the mixing angle α , besides M_A , $\tan\beta$, the slepton and chargino/neutralino parameters. In a full calculation M_h and α will be derived from the dressed (h^0, H^0) propagator system and thus are provided automatically in a comprehensive one-loop program. The simplified approach corresponds roughly to a situation where the scalar top system has masses around m_t , i.e. $m_{\tilde{t}_1} \cdot m_{\tilde{t}_2} \cong m_t^2$, when no large corrections to neutral Higgs masses and couplings occur.

We discuss the two processes (Z) and (A) separately:

$$e^+e^- \rightarrow Zh^0:$$

In order to exhibit the size of the box contribution we show in Fig. 4 the relative correction δ_Z^{box} , eq. (16), in the differential cross section as function of the scattering angle θ for two energies, $\sqrt{s} = 200$ GeV and 500 GeV. For the scalar leptons a universal mass $m_{\tilde{\gamma}} = 100$ GeV

and no mixing is assumed, and the $\tilde{\chi}^0, \tilde{\chi}^+$ system is fixed by choosing $M = \mu = 150$ GeV. This corresponds to a mass of 76 GeV for the lightest $\tilde{\chi}^+$ and 44 GeV to the lightest $\tilde{\chi}^0$. The figure shows that the contribution reaches already -5% at 200 GeV for large $\tan\beta$, and increases remarkably to $-(20 \div 25)\%$ at 500 GeV. It can be seen that the dominating piece is from the gauge and Higgs sector (2hdm), whereas the genuine SUSY boxes are smaller than 5%, also when we decrease the slepton masses to lower values close to the present experimental limit. This dominance of the gauge-Higgs part persists also at higher energies, as displayed in Figure 5 showing the integrated cross section as function of the c. m. energy. The dependence on the SUSY breaking parameters M, μ is visualized in Fig. 6, again for the integrated cross section: for increasing M and μ the genuine SUSY boxes become very small, as expected from decoupling properties, and we are left with the gauge-Higgs subclass of diagrams. As a consequence, the box contribution to $e^+e^- \rightarrow Zh$ is not very sensitive to the details of the SUSY sector, and is qualitatively very similar to the Standard Model situation [3].

$e^+e^- \rightarrow A^0h^0$:

In Fig. 7 we show the relative correction δ_A^{box} (eq. 16), with the same parameter choices as in Fig. 4. The contribution of the box diagrams to the process (A) are somewhat smaller than to the process (Z): at $\sqrt{s} = 200$ GeV the relative correction is about 2% and reaches nearly 10% at 500 GeV. Again the contributions of the gauge and Higgs sector dominate. The effect of diagrams containing genuine SUSY particles is less than $0.5 \div 1\%$ for $m_{\tilde{\gamma}} = 100$ GeV and slightly larger for $m_{\tilde{\gamma}} = 50$ GeV. The dependence of the integrated cross section on the c. m. energy \sqrt{s} is plotted in Fig. 8. As can be seen, the effects of genuine SUSY diagrams decrease with \sqrt{s} . We also show the dependence on M and μ in Fig. 9: the behaviour is similar to the case of the Zh^0 production, i.e. the SUSY boxes become very small with increasing SUSY breaking parameters.

In summary, the box diagrams yield a sizable contribution to the differential and integrated Higgs production cross sections, in particular in the energy domain of a next linear e^+e^- collider.

References

- [1] For a recent review see:
M. Felcini, ETHZ–IPR–94–11–REV (December 1994), to appear in the Proceedings of the Zeuthen Workshop on Elementary Particle Physics “Physics at LEP200 and beyond”, Teupitz, April 1994.
- [2] see “Higgs Particles”, in: e^+e^- Collisions at 500 GeV, DESY 92–123A,B; DESY 93–123C, ed.: P.M. Zerwas.
- [3] J. Fleischer, F. Jegerlehner: *Nucl. Phys.* **B 216** (1983) 469.
A. Denner, J. Kübelbeck, R. Mertig, M. Böhm: *Z. Phys.* **C 55** (1992) 605.
B.A. Kniehl: *Z. Phys.* **C 55** (1992) 605.
- [4] J. Ellis, G. Ridolfi, F. Zwirner, *Phys. Lett.* **257 B** (1991) 83
J. Ellis, G. Ridolfi, F. Zwirner, *Phys. Lett.* **262 B** (1991) 477
Y. Okada, M. Yamaguchi, T. Yanagida, *Phys. Lett.* **262 B** (1991) 54
J.L. Lopez, D.V. Nanopoulos, *Phys. Lett.* **266 B** (1991) 397
A. Brignole, J. Ellis, G. Ridolfi, F. Zwirner, *Phys. Lett.* **271 B** (1991) 123
- [5] R. Barbieri, M. Frigeni, *Phys. Lett.* **258 B** (1991) 395
R. Barbieri, M. Frigeni, F. Caravaglios, *Phys. Lett.* **258 B** (1991) 167
J.R. Espinosa, M. Quiros, *Phys. Lett.* **266 B** (1991) 389
K. Sasaki, M. Carena, C.E.M. Wagner, *Phys. Rev. Lett.* **381** (1992) 66
H.E. Haber, R. Hempfling, *Phys. Rev.* **D 48** (1993) 4280
- [6] P.Chankowski, S. Pokorski, J. Rosiek, *Nucl. Phys.* **B 423** (1994) 437; **B 423** (1994) 497.
- [7] A. Sopczak, *Int. J. Mod. Phys.* **A 9** (1994) 1747.
- [8] J. Rosiek, A. Sopczak, P. Chankowski, S. Pokorski, in: “ e^+e^- Collisions at 500 GeV: the Physics Potential”, DESY 93–123C, ed.: P.M. Zerwas;
J. Rosiek, A. Sopczak, CERN–PPE/94–134.
- [9] J.F. Gunion, H.E. Haber, G. Kane, S. Dawson: The Higgs Hunter’s Guide, Addison – Wesley 1990.
H.E. Haber, G. Kane: *Phys. Reports* **C 117** (1985) 75.
- [10] A. Denner, H. Eck, O. Hahn, J. Kübelbeck: *Nucl. Phys.* **B 387** (1992) 467.
- [11] J.A.M. Vermaseren: FORM, 1989.
- [12] G.J.van Oldenborgh: NIKHEF-H/90-15.

Figures

- **Fig.1** Born diagrams contributing to $e^+e^- \rightarrow Z^0h^0$ and $e^+e^- \rightarrow A^0h^0$.
- **Fig.2** Box diagrams contributing to $e^+e^- \rightarrow Z^0h^0$.
- **Fig.3** Box diagrams contributing to $e^+e^- \rightarrow A^0h^0$.
- **Fig.4** Relative box contribution δ_Z^{box} for $e^+e^- \rightarrow Z^0h^0$ at $\sqrt{s} = 200$ GeV, 500 GeV and $\tan\beta = 2, 50$.
- **Fig.5** Relative box contribution Δ_Z^{box} for $M = \mu = 150$ GeV.
If curves are marked by ‘-se’ etc. $-\Delta_{Z,A}^{se}$ is plotted.
- **Fig.6** Δ_Z^{box} at $\sqrt{s} = 200$ GeV, 500 GeV and $\tan\beta = 2, 50$.
- **Fig.7** Relative box contribution δ_A^{box} for $e^+e^- \rightarrow A^0h^0$ at $\sqrt{s} = 200$ GeV, 500 GeV and $\tan\beta = 2, 50$.
- **Fig.8** Relative box contribution Δ_A^{box} for $M = \mu = 150$ GeV.
- **Fig.9** Δ_A^{box} at $\sqrt{s} = 200$ GeV, 500 GeV and $\tan\beta = 2, 50$.

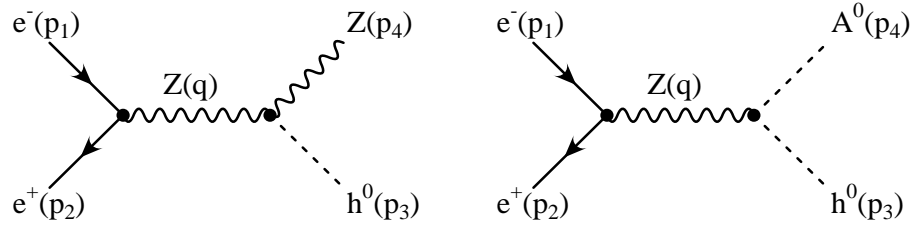


Figure 1

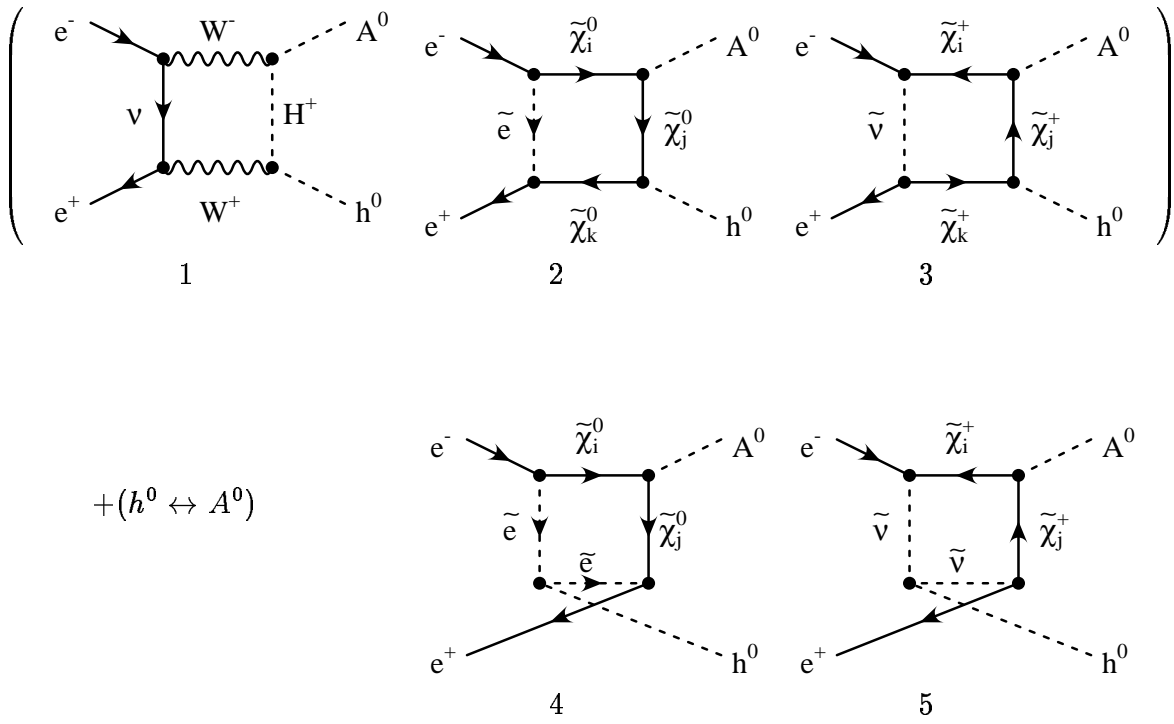


Figure 3

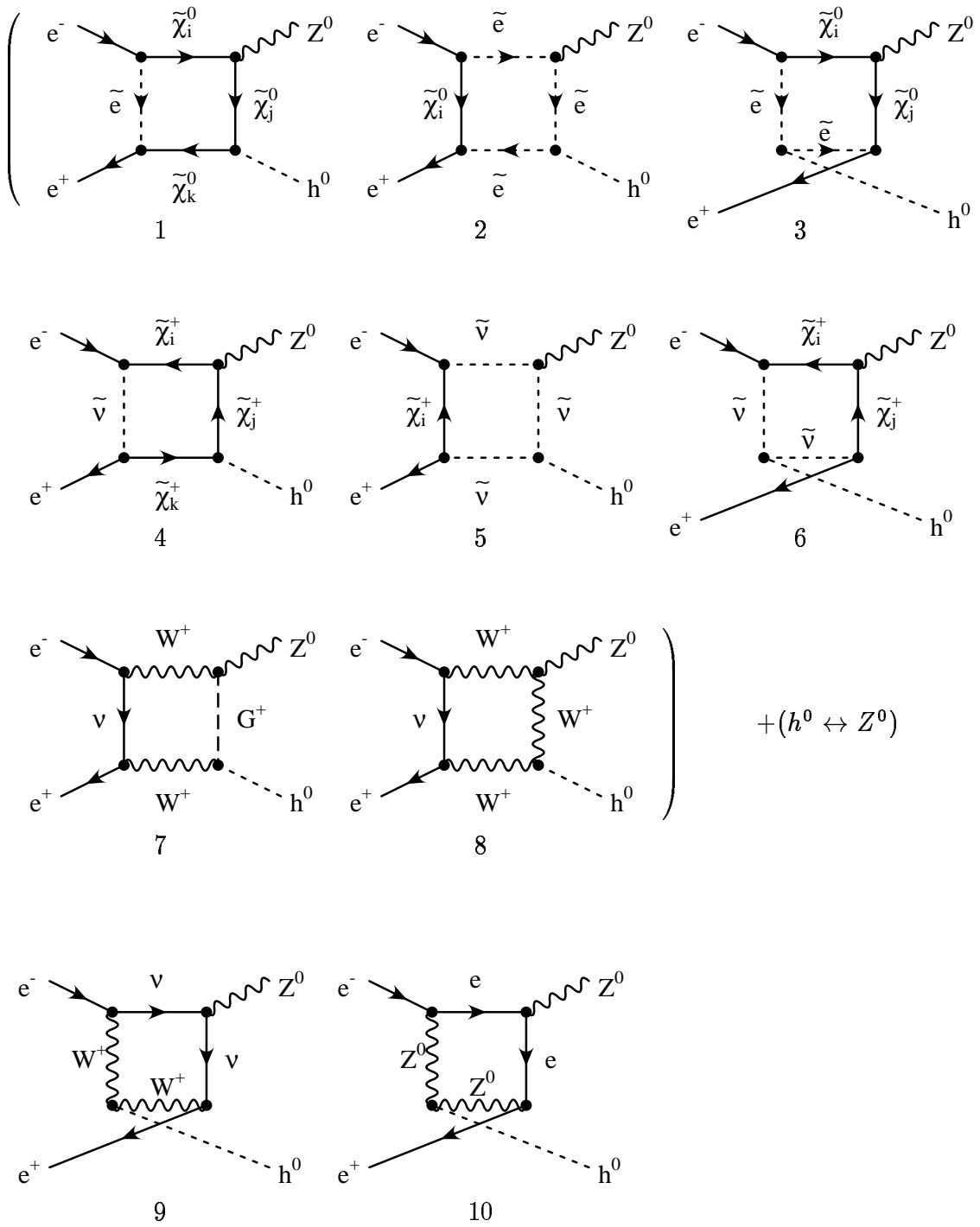


Figure 2

$e^+e^- \rightarrow Z^0 h^0$, $M_{\text{susy}} = \mu = 150\text{GeV}$, $m_A = 90\text{GeV}$, 100GeV sfermions

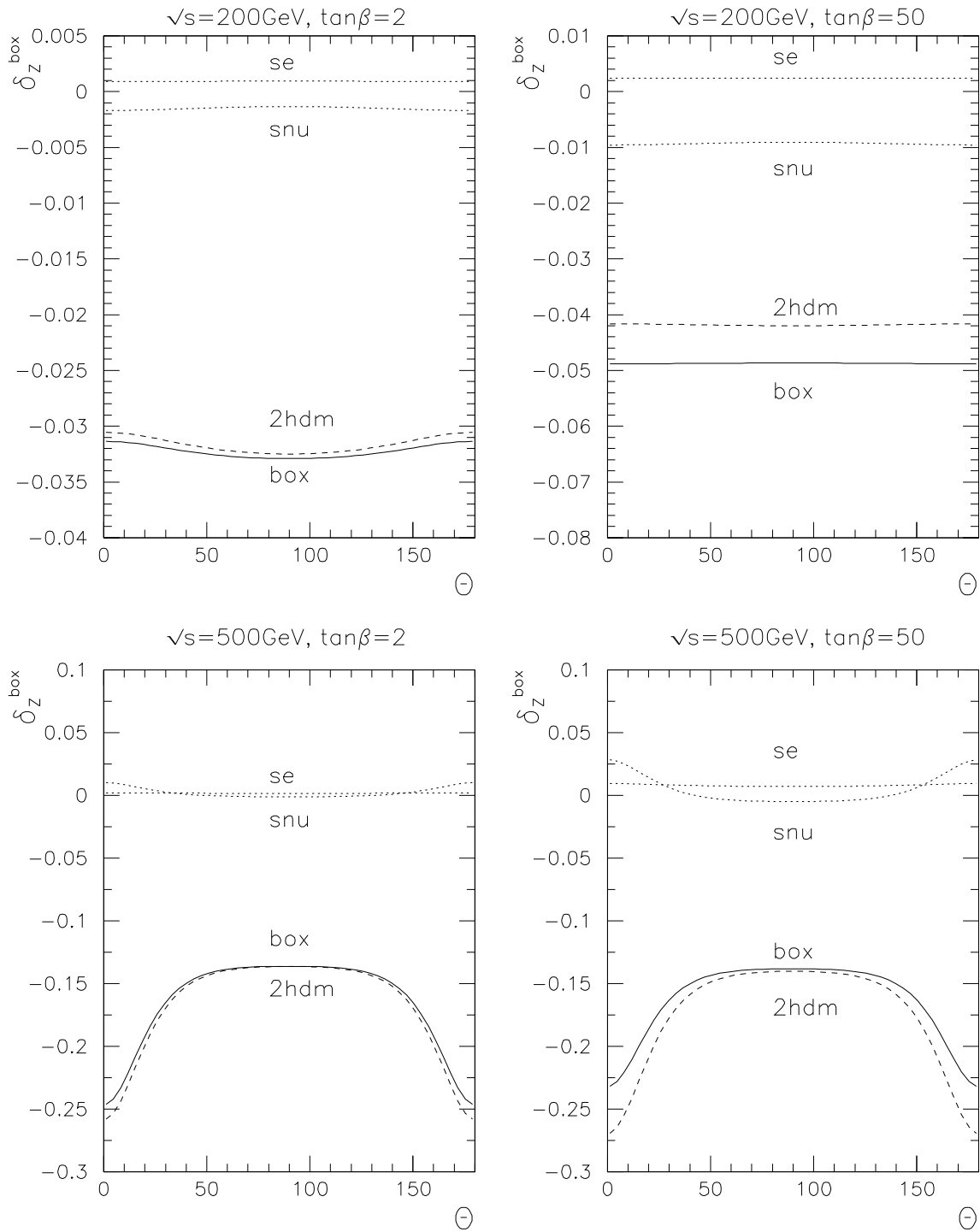


Figure 4

$e^+e^- \rightarrow Z^0 h^0$, $M_{\text{susy}} = \mu = 150 \text{ GeV}$, $m_A = 90 \text{ GeV}$, 100 GeV sfermions

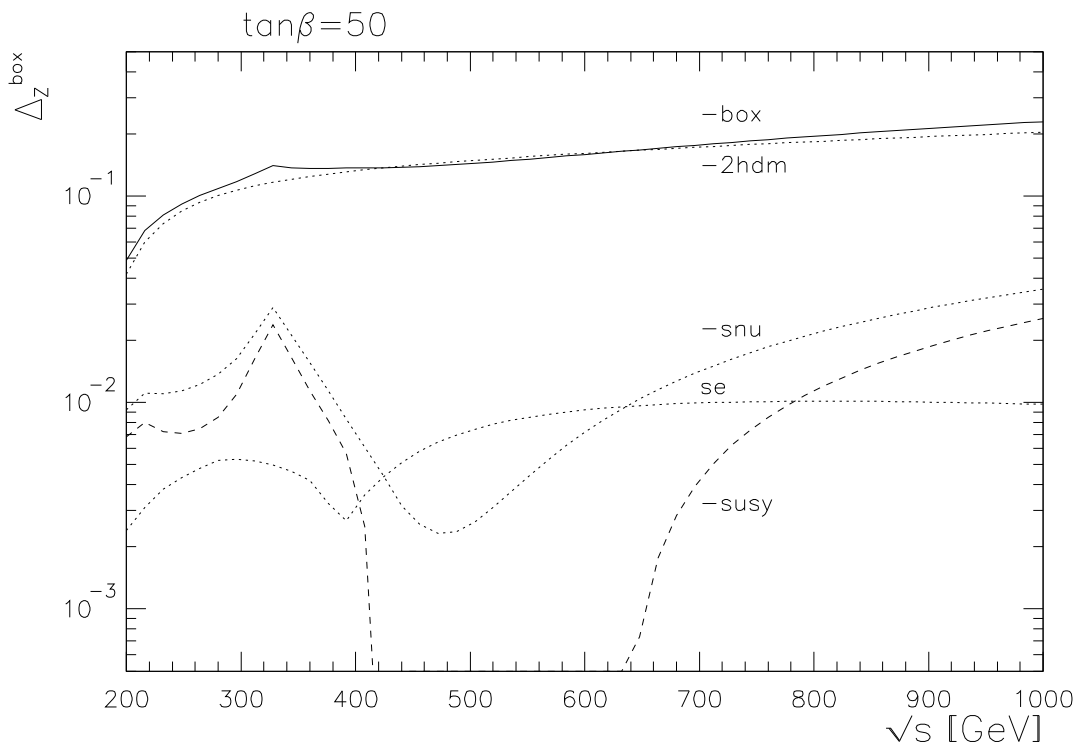
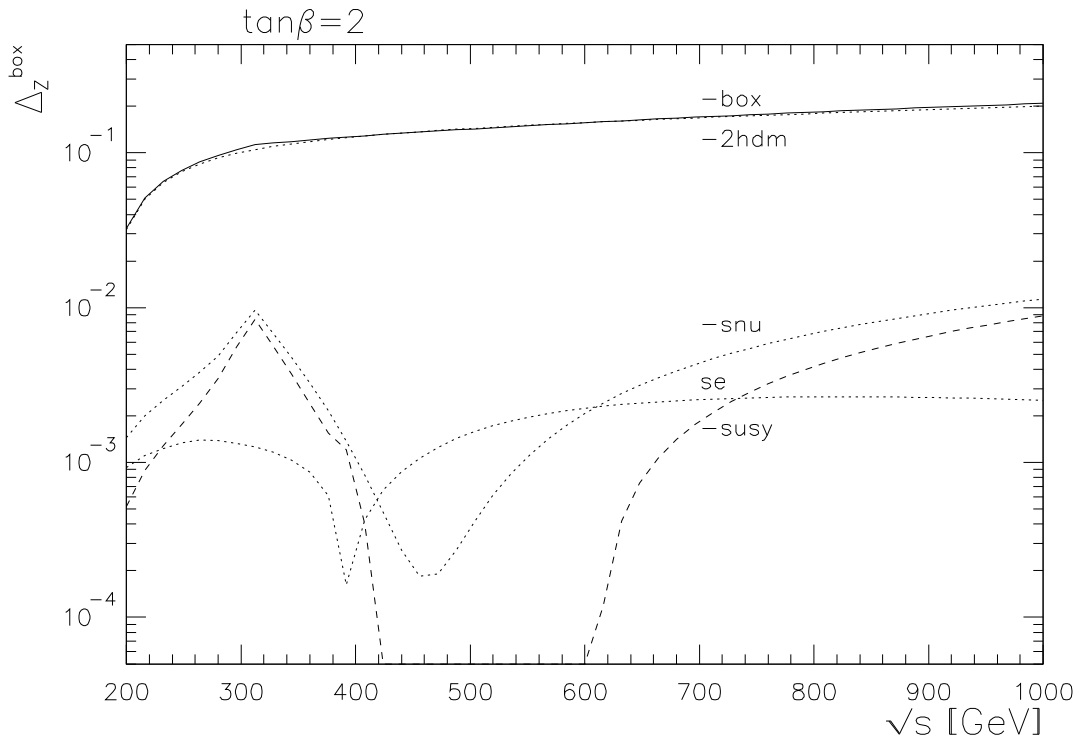


Figure 5

$$e^+e^- \rightarrow Z^0 h^0, \quad m_A=90\text{GeV}, \quad m_{S1}=100\text{GeV}$$

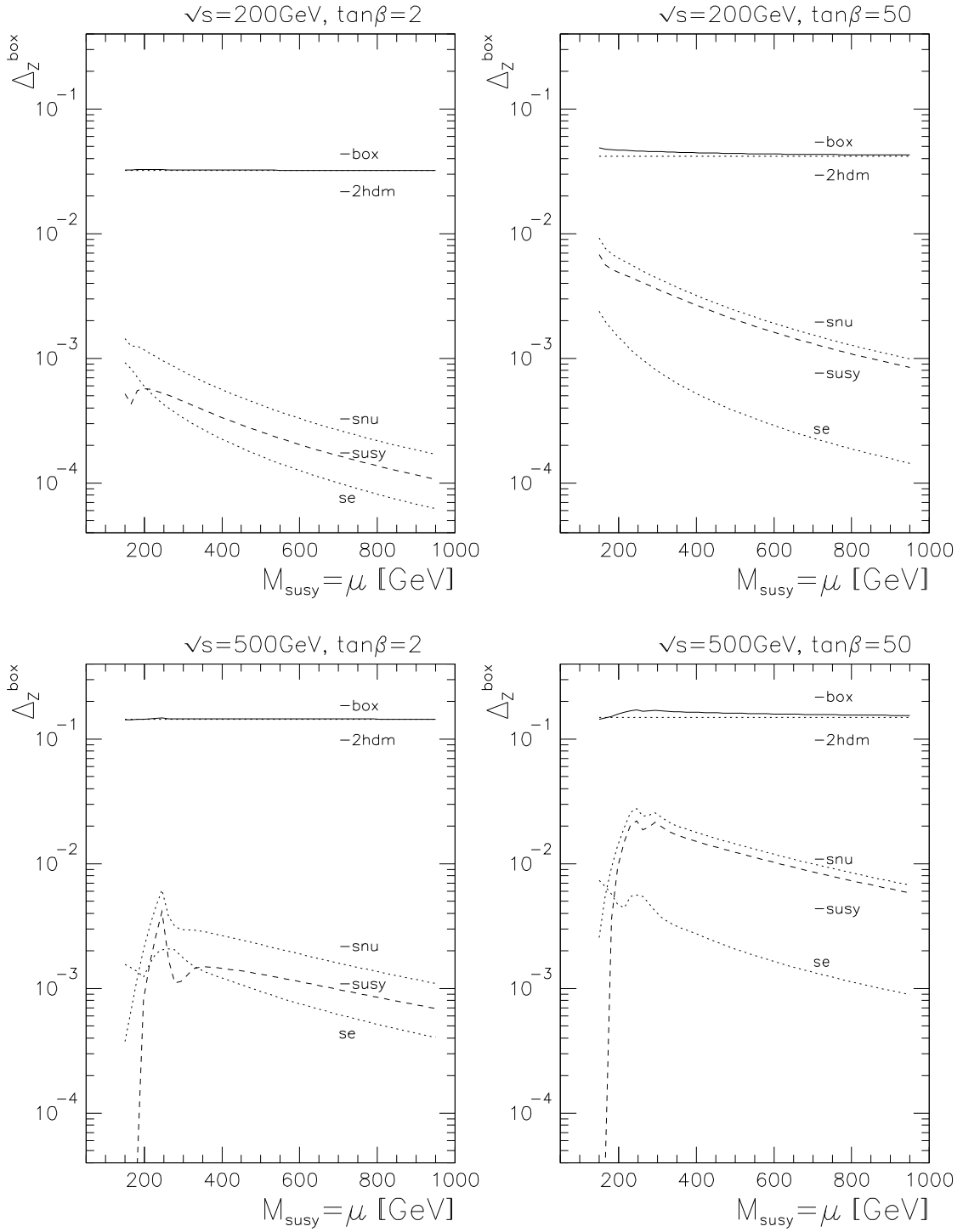


Figure 6

$e^+e^- \rightarrow A^0h^0$, $M_{\text{susy}}=\mu=150\text{GeV}$, $m_A=90\text{GeV}$, 100GeV sfermions

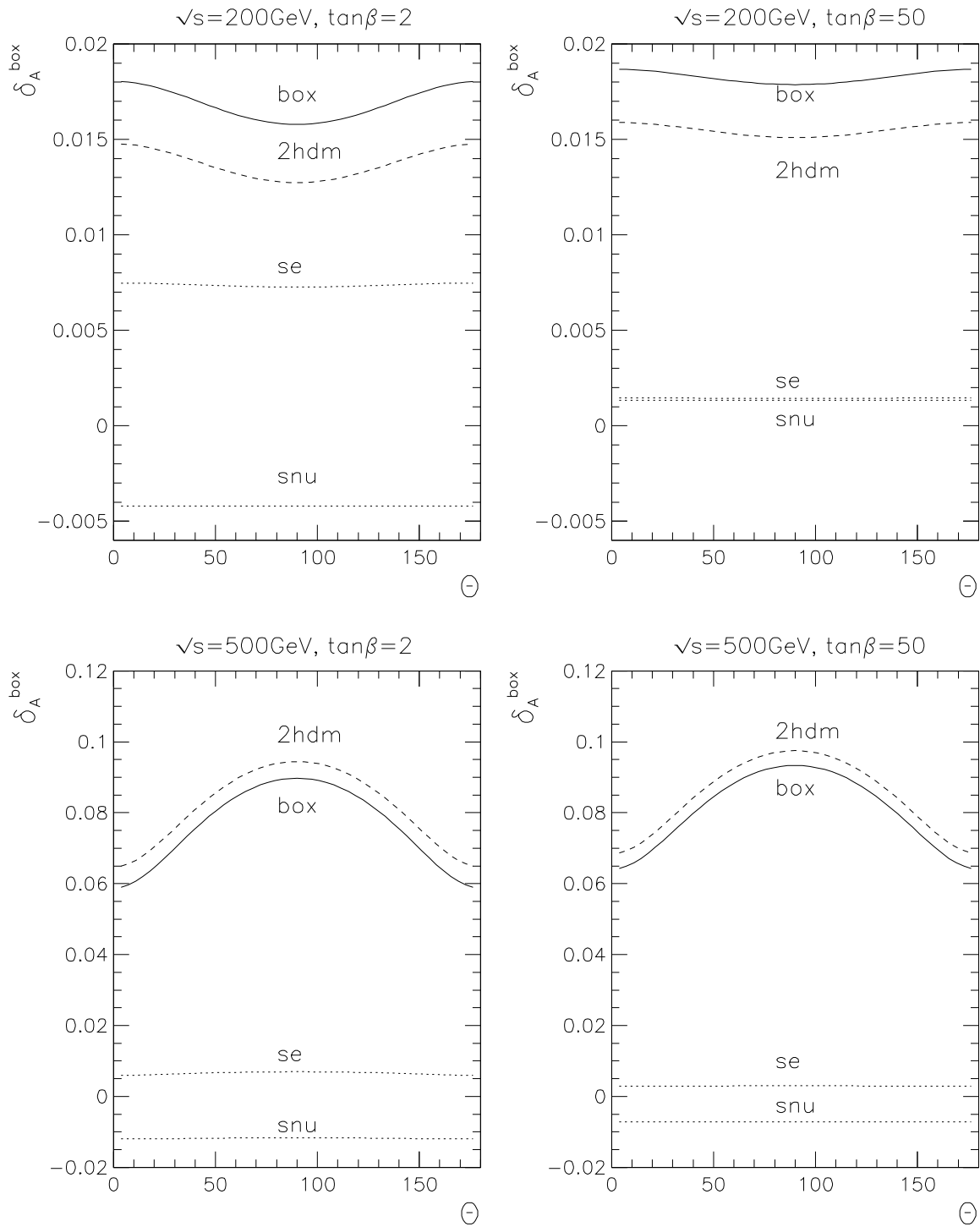


Figure 7

$e^+e^- \rightarrow A^0h^0$, $M_{\text{susy}}=\mu=150\text{GeV}$, $m_A=90\text{GeV}$, 100GeV sfermions

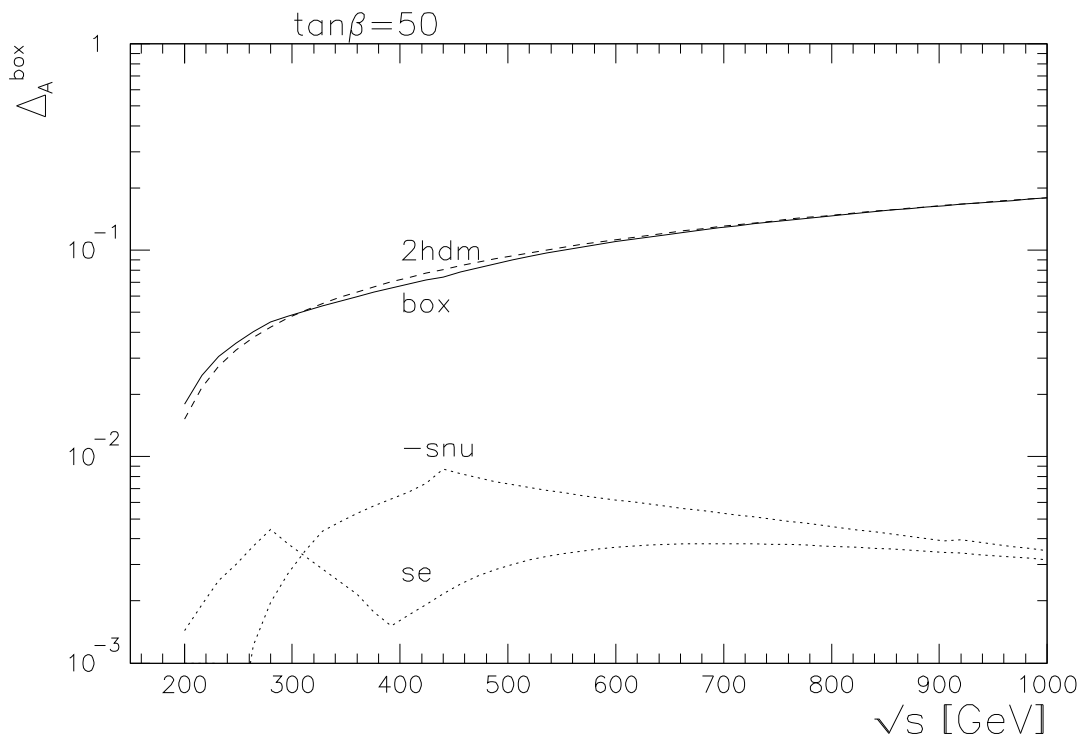
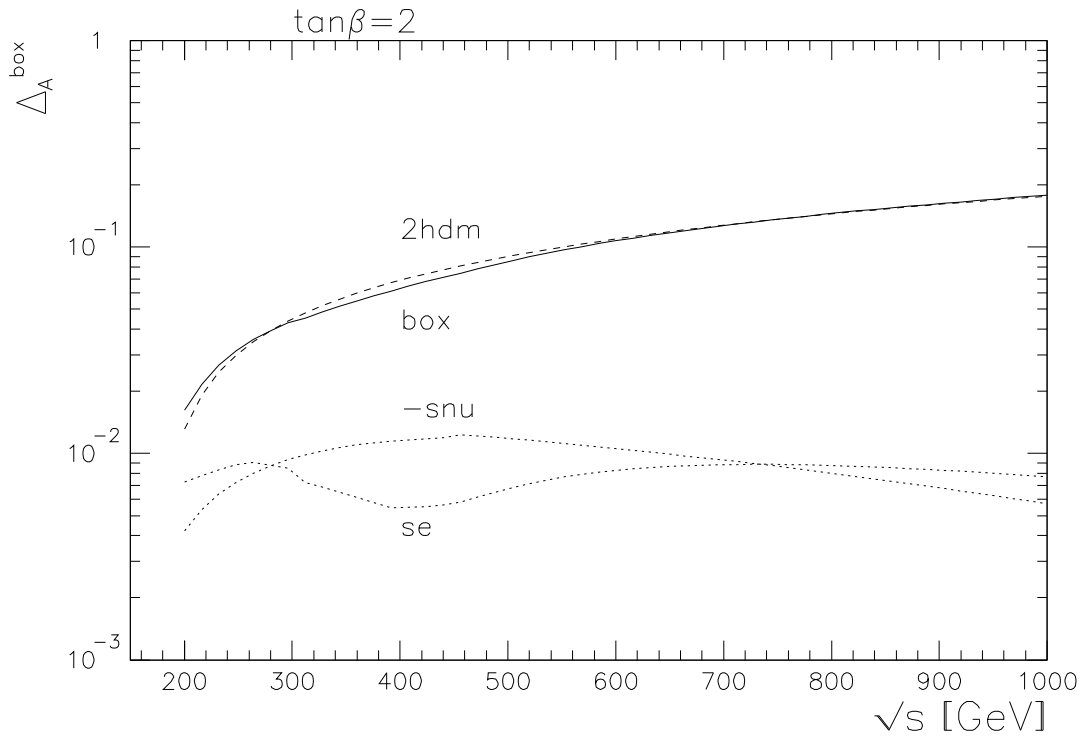


Figure 8

$e^+e^- \rightarrow A^0h^0$, $m_A=90\text{GeV}$, box: solid, 2hdm: dashed, $m_{\text{SI}}=100\text{GeV}$

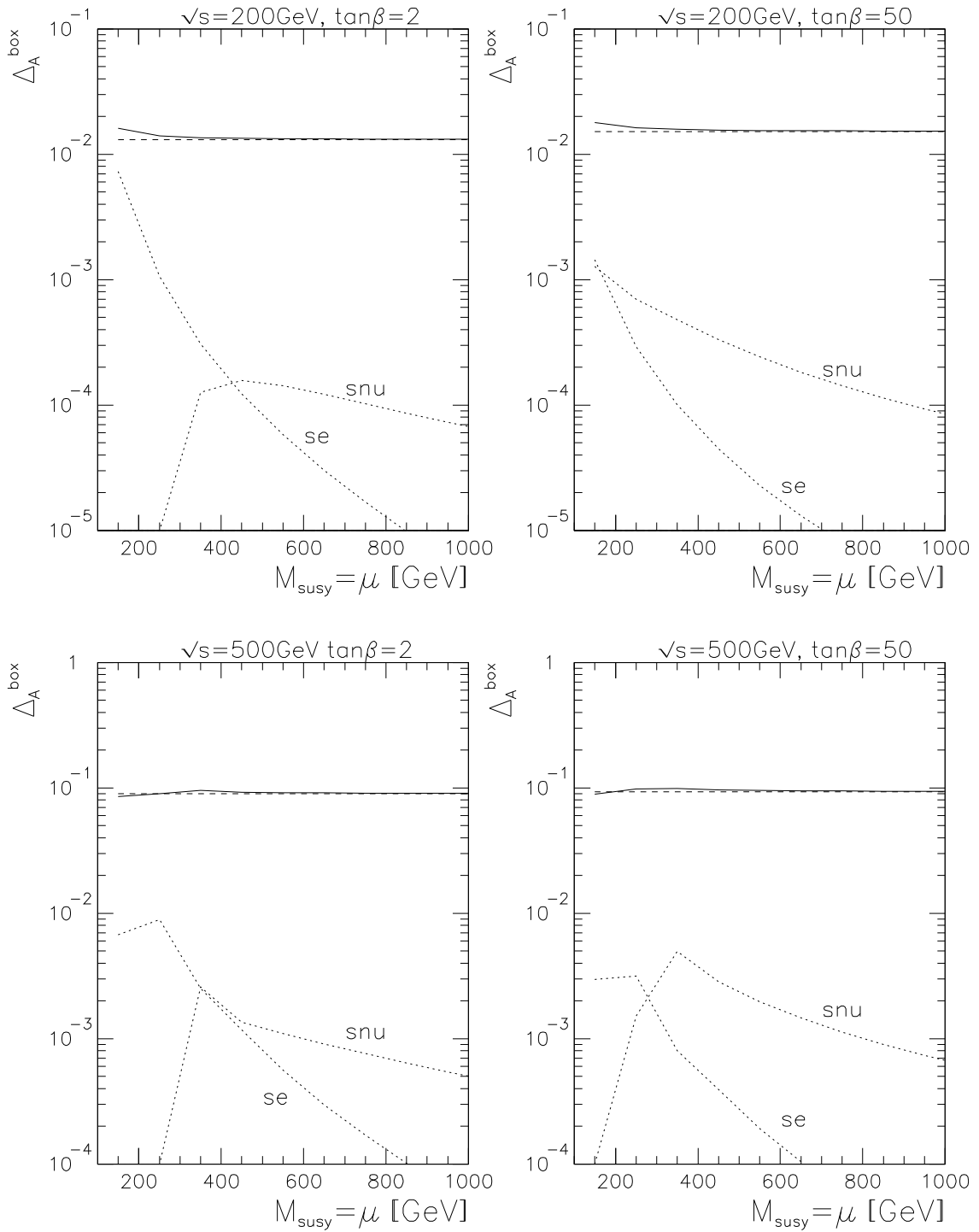


Figure 9